SUPPLEMENTAL INFORMATION

Membrane fluidity adjusts the insertion of the transacylase PlsX to regulate phospholipid biosynthesis in Gram-positive bacteria

Diego E. Sastre[1*], Luis G. M. Basso[2], Beatriz Trastoy[3], Javier O. Cifuente[3], Xabier Contreras[4,5], Frederico Gueiros-Filho[6], Diego de Mendoza[7], Marcos V.A.S. Navarro[1], Marcelo E. Guerin[3,4*]

[1] Departamento de Biofísica Molecular, Instituto de Física de São Carlos, Universidade de São Paulo, São Carlos, São Paulo, Brasil.
[2] Departamento de Física, Faculdade de Filosofia Ciências e Letras de Ribeirão Preto, Universidade de São Paulo, Ribeirão Preto, São Paulo, Brasil
[3] Structural Biology Unit, CIC bioGUNE Technological Park of Bizkaia, Derio, Vizcaya, Spain.
[4] IKERBASQUE, Basque Foundation for Science, 48013 Bilbao, Spain
[5] Instituto Biofisika, Consejo Superior de Investigaciones Científicas – Universidad del País Vasco/Euskal Herriko Unibertsitatea (CSIC,UPV/EHU), Barrio Sarriena s/n, Leioa, 48940 Bizkaia, Spain; Departamento de Bioquímica, Universidad del País Vasco, Leioa, 48940 Bizkaia, Spain.
[6] Departamento de Bioquímica, Instituto de Química, Universidade de São Paulo, São Paulo, São Paulo, Brasil.
[7] Instituto de Biología Molecular y Celular de Rosario (IBR), Rosario, Santa Fe, Argentina.

Running title: *Phospholipid biosynthesis regulation in Gram-positve bacteria*

[*]**To whom correspondence should be addressed:** Diego E. Sastre, Departamento de Biofísica Molecular, Instituto de Física de São Carlos, Universidade de São Paulo, Av. João Dagnone 1100, CEP 13563-120, São Carlos, SP, Brasil. E-mail: diegosastre82@gmail.com; Marcelo E. Guerin, Structural Biology Unit, CIC bioGUNE, Bizkaia Technology Park, 48160, Derio, Spain, mrcguerin@cicbiogune.es

Keywords: phospholipid biosynthesis, membrane binding, membrane insertion, membrane fluidity, protein-lipid interaction, Gram-positive bacteria.

SUPPLEMENTARY FIGURES

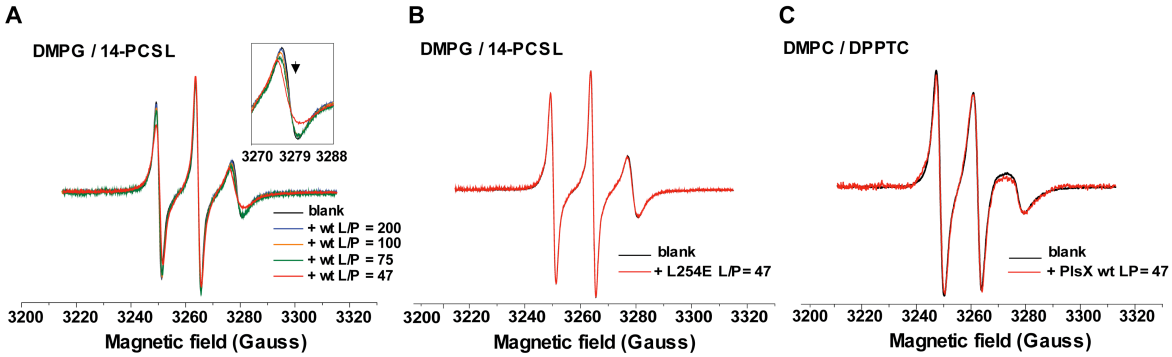

Figure S1. Lineshape ESR spectral changes promoted by the PlsX wt and PlsX^{L254E} mutant. *A*. ESR spectra of 14-PCSL in DMPG SUVs in the absence (black) and presence (red) of PlsX wt at different lipid-to-protein (L/P) molar ratios obtained at 30°C. ***B.*** ESR spectra of 14-PCSL in DMPG SUVs in the absence (black) and presence (red) of PlsX^{L254E} at 1:47 protein-to-lipid molar ratio obtained at 30°C. ***C.*** ESR spectra of head group spin label DPPTC in DMPC SUVs in the absence (black) and presence (red) of PlsX wt at 1:47 protein-to-lipid molar ratio at 30°C (fluid phase).

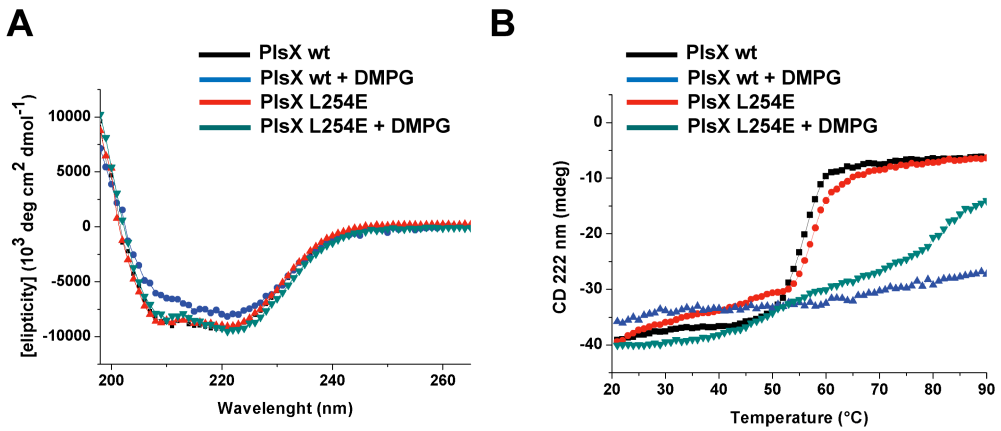

Figure S2. PlsX^{L254E} mutant perturb membrane interaction. *A*. The far-UV CD of PlsX and PlsX^{L254E} were recorded at 20°C in the absence and presence of DMPG. *B*. The thermal induced unfolding of PlsX and PlsX^{L254E} in the absence and presence of DMPG, were assessed by monitoring the thermal dependence of the ellipticity at 222 nm.

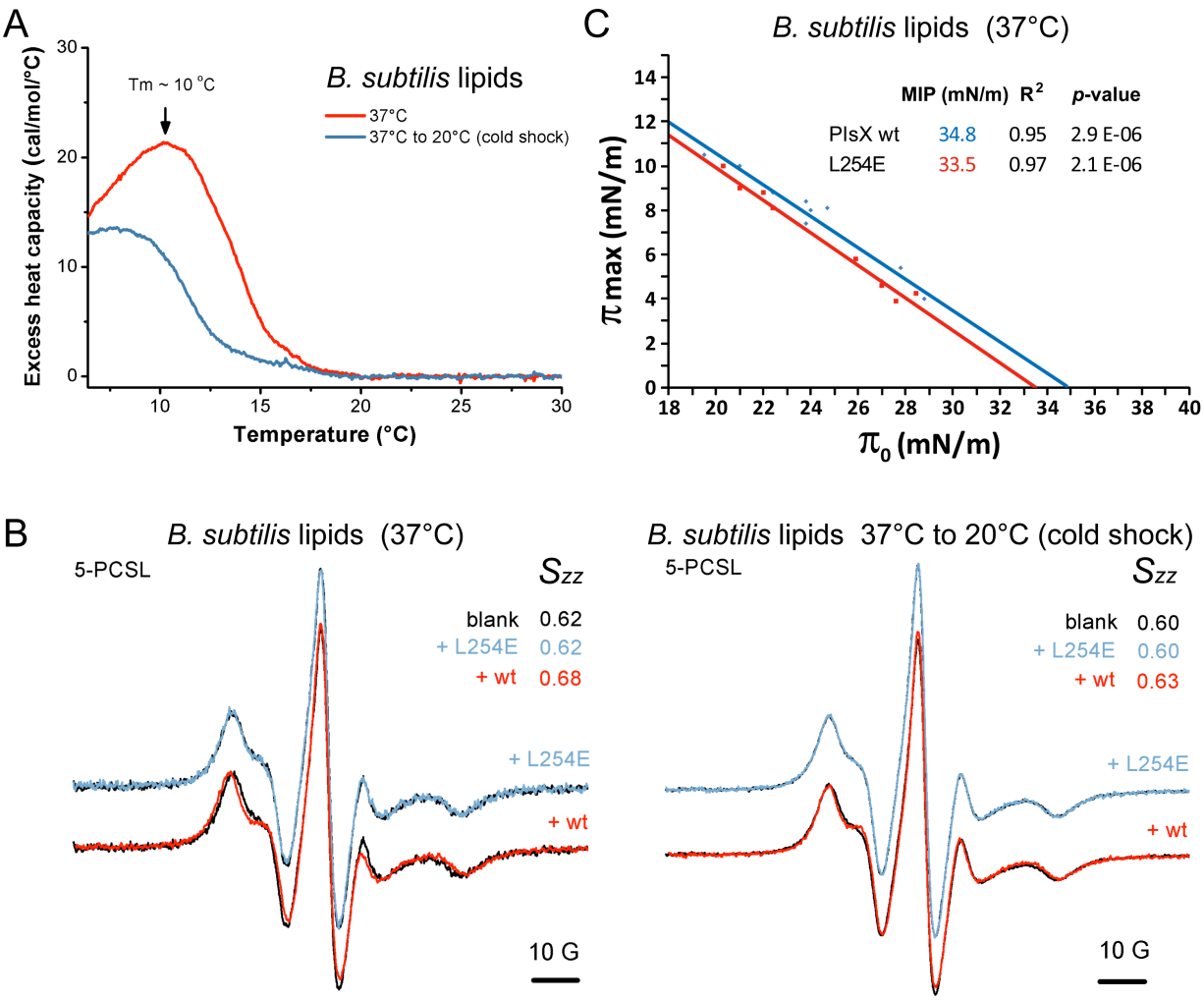

Figure S3. Analysis of PlsX wt and PlsX^{L254E} mutant insertion to membrane lipids extracted from *B. subtilis* cells *A*. Representative DSC thermograms obtained for small unilamellar vesicles (SUVs) comprised of membrane lipids isolated from *B. subtilis* PY79 cells at 37 °C and after a cold shock (from 37°C to 20 °C) were used to measure the apparent phase transition temperature (T_m). The Tm of the 37°C-grown cell lipid membranes was about 10°C, whereas that obtained with the lipids from cells grown after a cold shock was clearly lower (not determined due to technical limitations of the instrument). *B*. ESR experiments were performed using SUVs composed of membrane lipids extracted from *B. subtilis* PY79 cells grown at 37°C (right panel) and after a cold shock (left panel). ESR spectra of 5-PCSL, in *B. subtilis* lipids SUVs in the absence (black) and presence of PlsX (red) or PlsX^{L254E} (blue) at 1:50 protein-to-lipid molar ratio were obtained at 25 °C (fluid phase). The order parameter S_{zz} was calculated as previously described (30). *C*. Langmuir films assays using monolayers made of membrane lipids from *B. subtilis* cells grown at 37°C were performed at 30°C (fluid phase). At least nine data points were used to generate statistical significant linear regression to obtain the maximum insertion pressure (MIP) values for each condition.

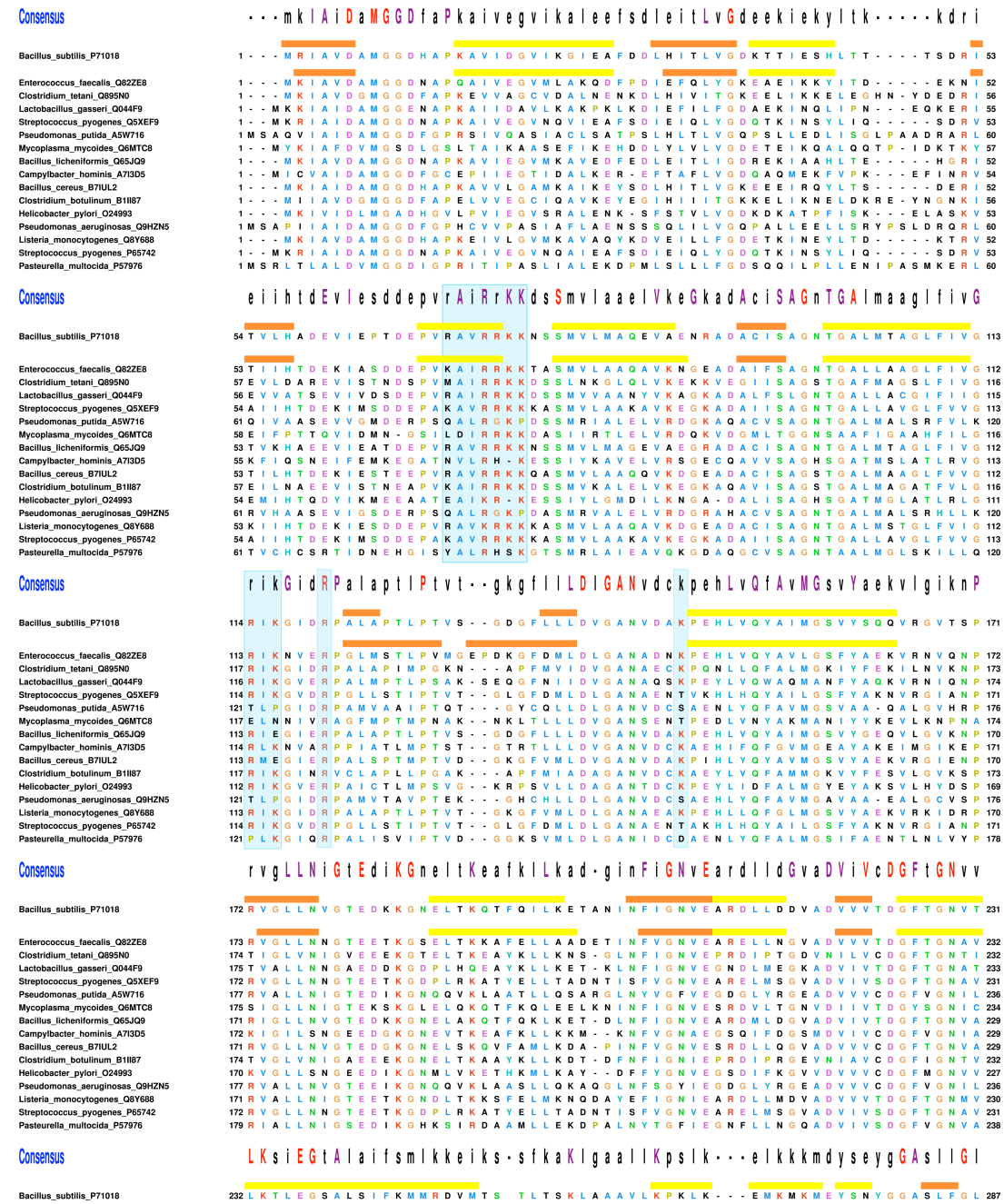
Consensus
Bacillus_subtilis_P71018
Enterococcus_faecalis_Q82ZE8
Clostridium_tetani_Q895N0
Lactobacillus_gasseri_Q044F9
Streptococcus_pyogenes_Q5XEF9
Pseudomonas_putida_A5W716
Mycoplasma_mycoides_Q6MTC8
Bacillus_licheniformis_Q65JQ9
Campylbacter_hominis_A7I3D5
Bacillus_cereus_B7IUL2
Clostridium_botulinum_B1II87
Helicobacter_pylori_O24993
Pseudomonas_aeruginosas_Q9HZN5
Listeria_monocytogenes_Q8Y688
Streptococcus_pyogenes_P65742
Pasteurella_multocida_P57976

Figure S4. PlsX structural alignment with selected bacterial homologs. Residues are indicated in one-letter Clustal X coloring scheme. The consensus sequence highlights highly conserved residues in capitalized one-letter code (100% conserved residues in red, purple colored conservation ≥ 80%). Orange and green bars indicates either α-helices and β-strand regions present in the crystal structure of PlsX from *B. subtilis* (pdb code 1VI1) and the reported crystal structure of PlsX from *E. faecalis* (pdb code 1U7N). The light blue background boxes indicates the region corresponding to the positively charged patch, presumed ACP-binding site.

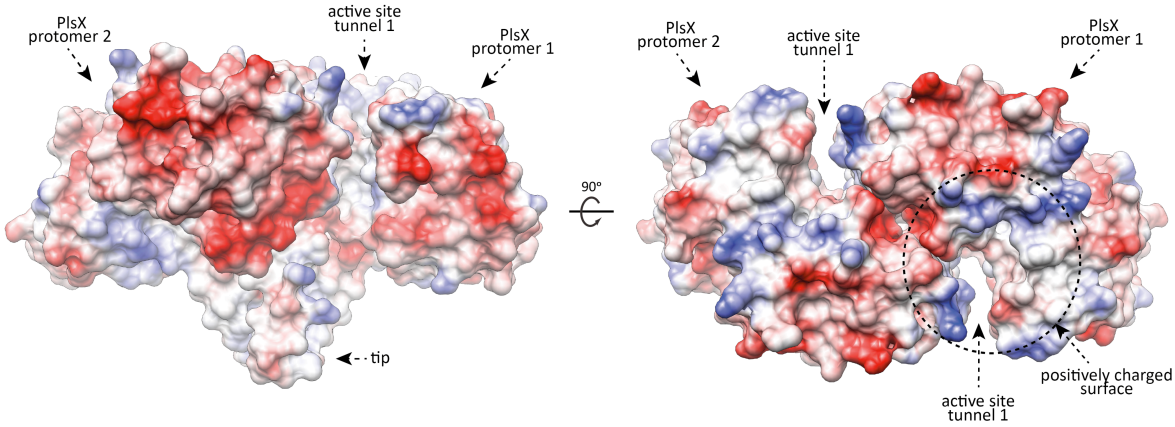

Figure S5. A conserved positively charged patch at the surface of PlsX. Two views of the electrostatic surface representation of PlsX from B. *subtilis*, showing the positively charged, surface exposed region.

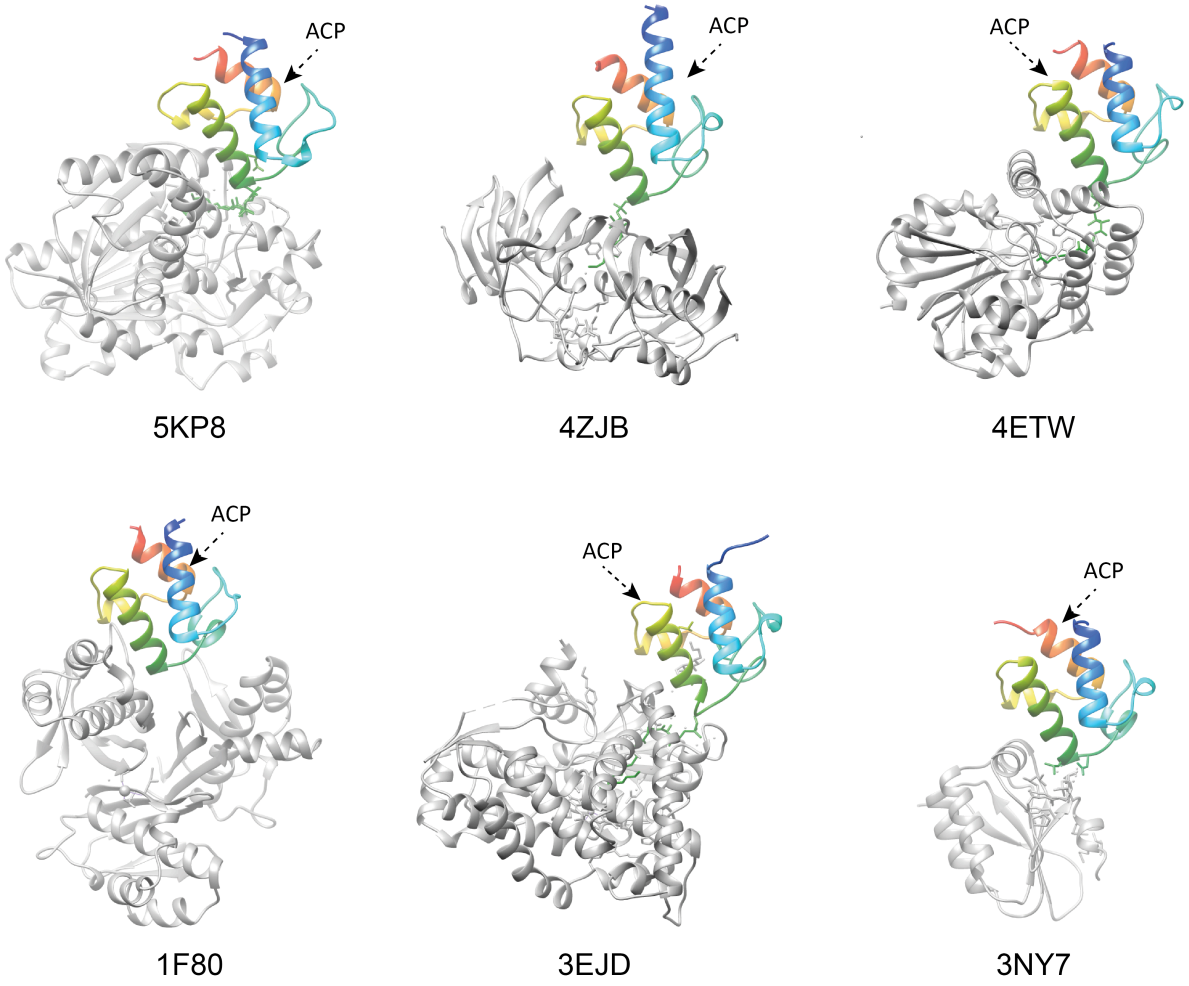

Figure S6. Crystal structures of ACP-enzyme complexes. ACP preferentially orientates to bind different enzyme partners. 5KP8, HMG synthase in complex with acetyl-ACP; 4ZJB, FabZ in complex with holo-ACP; 4ETW, BioH in complex with pimeloyl-ACP methyl ester; 1F80, ACP synthase in complex with holo-ACP; 3EJD, P450BioI in complex with acyl-ACP; 3NY7, STAS domain of YchM in complex with ACP.

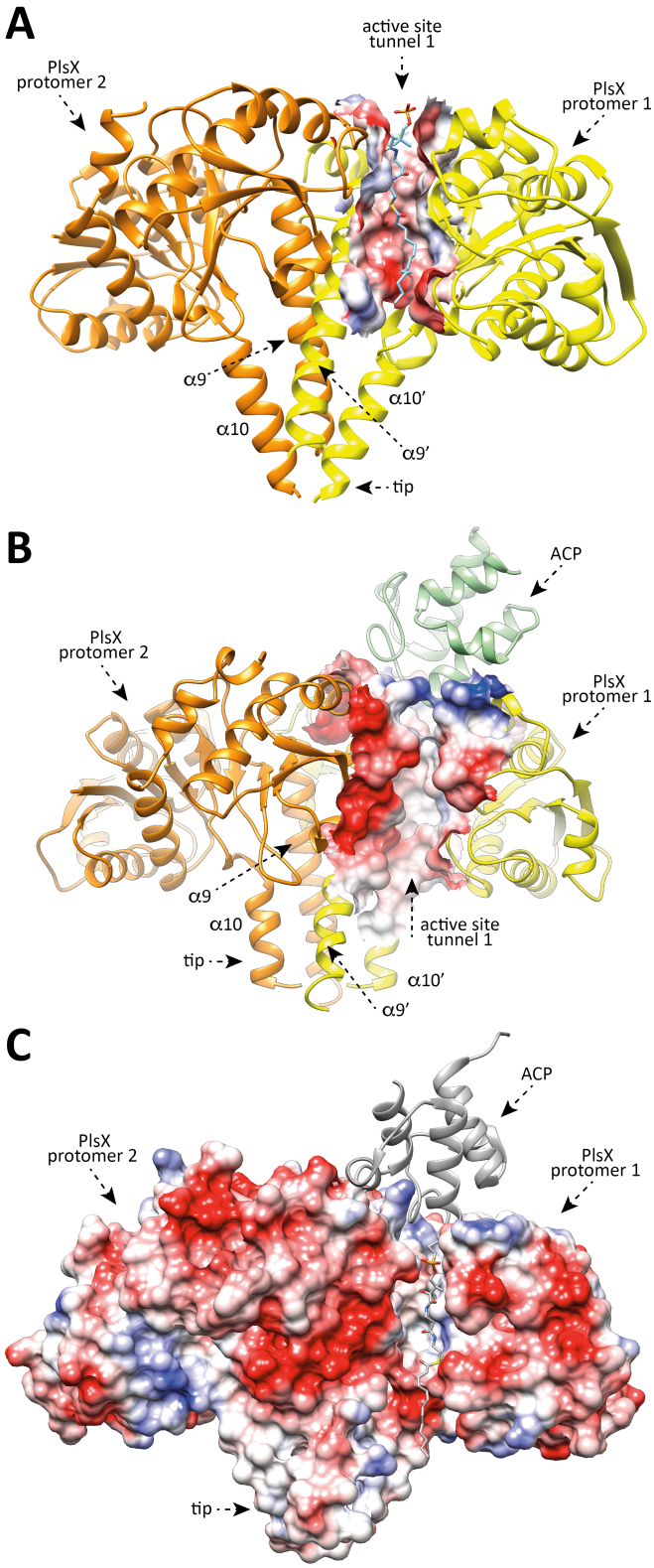

Figure S7. The 4'-phosphopantetheine myristate and ACP binding sites. *A*. Docking calculations in which a 4'-phosphopantetheine myristate molecule attaches to the main groove of protomer 2 of PlsX. *B*. Docking calculations in which an ACP molecule attaches to the positively charged surface of PlsX. *C*. A proposed model for the PlsX-acyl-ACP complex.

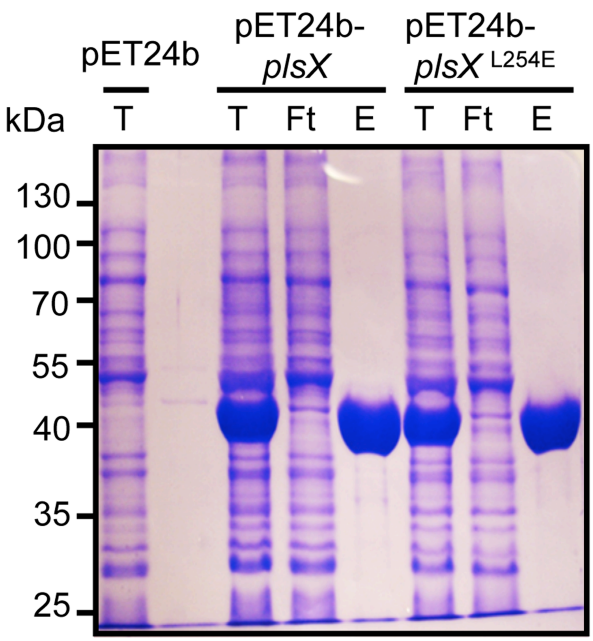

Figure S8. SDS-PAGE analyses of PlsX wt and PlsX^{L254E} protein purification. *E. coli* BL21 cells containing the empty vector pET24 or pET24-*pls*X wt or pET24b-*pls*X^{L254E} were pelleted and the Total extract (T), Flow-through from Ni-agarose resin (Ft) and Elution of Nickel column (E) were loaded into 12% SDS-PAGE.

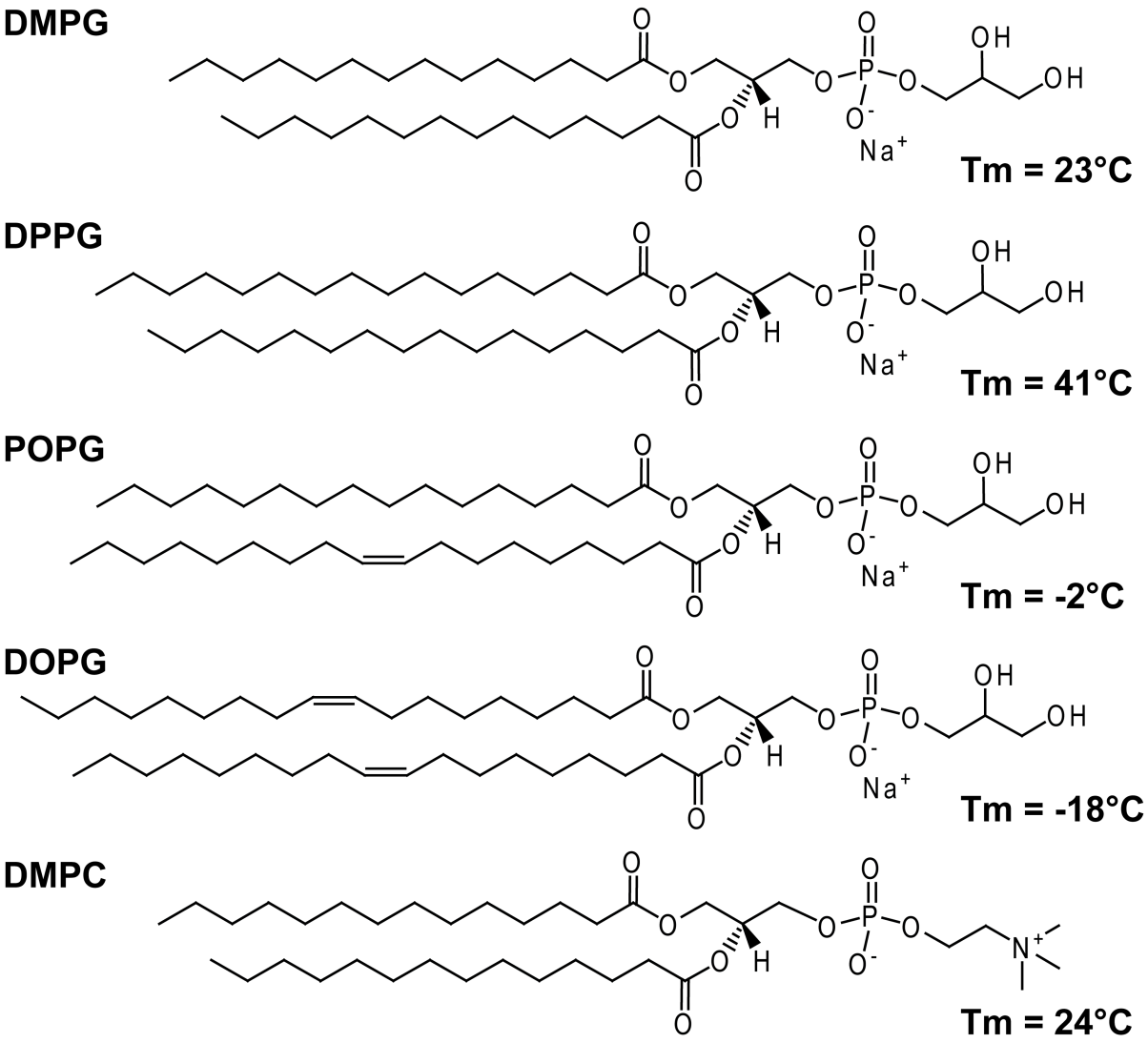

Figure S9. Chemical structure and melting temperatures of the phospholipids utilized in this work.